Article:
Andersson, ME, Verronen, PT, Marsh, DR et al. (2018) Polar Ozone Response to Energetic Particle Precipitation Over Decadal Time Scales: The Role of Medium-Energy Electrons. Journal of Geophysical Research: Atmospheres, 123 (1). pp. 607-622. ISSN: 2169-897X

https://doi.org/10.1002/2017JD027605

Polar ozone response to energetic particle precipitation over decadal time scales: the role of medium-energy electrons

M. E. Andersson[1], P. T. Verronen[1], D. R. Marsh[2], A. Seppälä[3,1], S-M. Päivärinta[1], C. J. Rodger[3], M. A. Clilverd[4], N. Kalakoski[1], and M. van de Kamp[1]

[1]Earth Observation, Finnish Meteorological Institute, Helsinki, Finland
[2]Atmospheric Chemistry Division, National Center for Atmospheric Research, Boulder, Colorado, USA
[3]Department of Physics, University of Otago, Dunedin, New Zealand
[4]British Antarctic Survey (NERC), Cambridge, UK

Key Points:

- Simulations (147 years) with new medium-energy electron forcing analyzed for chemical responses
- Middle mesospheric ozone is reduced by up to 20% on average by inclusion of MEE forcing
- Upper stratospheric ozone varies by up to 7% in the SH due to energetic particle precipitation

Corresponding author: P. T. Verronen, pekka.verronen@fmi.fi

Abstract

One of the key challenges in polar middle atmosphere research is to quantify the total forcing by energetic particle precipitation (EPP) and assess the related response over solar cycle time scales. This is especially true for electrons having energies between about 30 keV and 1 MeV, so-called medium-energy electrons (MEE), where there has been a persistent lack of adequate description of MEE ionization in chemistry-climate simulations. Here we use the Whole Atmosphere Community Climate Model (WACCM) and include EPP forcing by solar proton events, auroral electron precipitation, and a recently developed model of MEE precipitation. We contrast our results from three ensemble simulations (147 years) in total with those from the fifth phase of the Coupled Model Intercomparison Project (CMIP5) in order to investigate the importance of a more complete description of EPP to the middle atmospheric ozone, odd hydrogen, and odd nitrogen over decadal time scales. Our results indicate average EPP-induced polar ozone variability of 12–24% in the mesosphere, and 5-7% in the middle and upper stratosphere. This variability is in agreement with previously published observations. Analysis of the simulation results indicate the importance of inclusion of MEE in the total EPP forcing: In addition to the major impact on the mesosphere, MEE enhances the stratospheric ozone response by a factor of two. In the Northern Hemisphere, where wintertime dynamical variability is larger than in the Southern Hemisphere, longer simulations are needed in order to reach more robust conclusions.

1 Introduction

Variation in solar ultraviolet (UV) radiation is considered to be the main source of solar driven decadal variability in the stratosphere, influencing the ozone budget and radiative heating in the middle atmosphere [*Gray et al.*, 2010]. There is now growing evidence that solar driven energetic particle precipitation (EPP) is another important source for stratospheric variability [*Seppälä et al.*, 2014; *Matthes et al.*, 2017]. Auroral electron precipitation provides direct forcing at polar thermospheric altitudes (above about 100 km), while solar proton events (SPE) and medium-energy electron (MEE) precipitation generate excess ionization in the polar middle atmosphere (between about 30-80 km). This leads to significant changes in the neutral atmosphere through the formation of odd nitrogen (NO_x) and odd hydrogen (HO_x) [*Jackman et al.*, 2001; *Verronen et al.*, 2011; *Funke et al.*, 2011; *Andersson et al.*, 2012; *Fytterer et al.*, 2015; *Arsenovic et al.*, 2016]. Enhanced production

of NO_x and HO_x affects stratospheric and mesospheric ozone (O_3) [*Verronen et al.*, 2006; *Seppälä et al.*, 2007; *Jackman et al.*, 2008; *Andersson et al.*, 2014a], which then has the potential to further influence atmospheric dynamics [*Langematz et al.*, 2005; *Baumgaertner et al.*, 2011]. Simulations and analysis of meteorological data have given indications of chemical-dynamical coupling linking the initial EPP-induced response to changes in the lower atmosphere, and ground-level climate variations on a regional scale [*Lu et al.*, 2008; *Seppälä et al.*, 2009; *Baumgaertner et al.*, 2011; *Rozanov et al.*, 2012; *Seppälä et al.*, 2013]. It is possible that the impact of EPP on regional climate variability may be comparable or even exceeds the effects arising from solar UV variations [*Rozanov et al.*, 2005; *Seppälä and Clilverd*, 2014].

One of the outstanding challenges in understanding EPP impact on the atmosphere is the role of MEE in the total EPP forcing and the related atmospheric and climate response. There has been a persistent lack of an adequate description of MEE ionization in atmospheric simulations due to issues in the satellite-based precipitating flux observations [*Rodger et al.*, 2010a]. We know from satellite-based OH observations that there is a direct mesospheric response to MEE at geomagnetic latitudes between about 55 and 75 degrees [*Verronen et al.*, 2011; *Andersson et al.*, 2012; *Andersson et al.*, 2014b; *Zawedde et al.*, 2016]. Observations have further shown the resulting effect on mesospheric ozone, both in day-to-day changes during MEE events, and in longer-term variability [*Verronen et al.*, 2013; *Andersson et al.*, 2014a].

A major open question concerns the magnitude of the EPP-driven response in stratospheric ozone over decadal time scales [*Sinnhuber et al.*, 2006]. In order to have an impact, NO_x produced in the mesosphere-lower-thermosphere (MLT) region must be transported down to the upper stratosphere inside the polar vortex during wintertime when it is not destroyed by photolysis. NO_x descent has been observed during many winters [*Callis and Lambeth*, 1998; *Siskind et al.*, 2000; *Randall et al.*, 2009; *Päivärinta et al.*, 2013] and satellite data analysis has shown that NO_x descent occurs practically every winter, in both hemispheres, with significant inter-annual variability seen especially in the Northern Hemisphere (NH) [*Seppälä et al.*, 2007; *Funke et al.*, 2014a,b]. Capturing the observed magnitude of the NO_x descent has been difficult to simulate in models due to incomplete EPP forcing source producing the NO_x including, perhaps most importantly, the missing MEE ionization.

On a year-to-year basis, understanding the response of stratospheric ozone to the descending NO_x has been challenging because of the relatively large overall ozone variability due to atmospheric dynamics [*Päivärinta et al.*, 2013]. Nevertheless, from observations we know that polar upper stratospheric ozone can be depleted locally by 40–60% during winters of exceptionally strong NO_x descent [*Randall et al.*, 1998; *Randall et al.*, 2005]. A recent study using satellite data between 1979 and 2014 has revealed a long-term response of Southern Hemispheric (SH) stratospheric ozone to EPP activity, with an average ozone depletion of about 10–15% at 30–45 km altitude in late winter [*Damiani et al.*, 2016]. *Fytterer et al.* [2015] used a shorter time period of observations (2005–2010) and reported a 5–10% depletion of SH polar ozone at 25–50 km over the winter months.

Up to now there are been few simulations including MEE in some form [*Codrescu et al.*, 1997; *Semeniuk et al.*, 2011], but most recently *Arsenovic et al.* [2016] examined the MEE effect on the polar atmosphere using a chemistry-climate model. Although their MEE ionization data set restricted the simulated time period to just eight years, they nevertheless reported substantial MEE effects on polar stratospheric ozone and subsequently on atmospheric dynamics. However, for more general conclusions a multi-decadal time series of simulations is needed.

Here we use the Whole Atmosphere Community Climate Model (CESM1(WACCM)) to study the polar atmosphere response to EPP over decadal timescales. We present an extended simulation time series of 147 years (3×49 years ensemble of runs) which gives our results good statistical robustness. To complete the EPP forcing over the whole time series, we introduce to WACCM the new state-of-the-art MEE precipitation model which is part of solar forcing recommendation for the sixth phase of the Coupled Model Intercomparison Project CMIP6 [*van de Kamp et al.*, 2016; *Matthes et al.*, 2017]. The big open questions we wish to address concern the magnitude and detectability (e.g., statistical robustness) of EPP-driven signals in multi-decadal time series. These signals are currently unknown because most previous MEE studies have been restricted to time periods of $\sim$10 years or less. Thus, our study is an important contribution to the MEE research, and EPP research in general.

Note that we contrast our results to the simulations from the fifth phase of the Coupled Model Intercomparison Project (CMIP5) reported by *Marsh et al.* [2013] which were used for the fifth Intergovernmental Panel on Climate Change (IPCC) Assessment Report.

The CMIP5 simulations, which include no MEE forcing, are freely available to the community and are widely used. It is very important to establish if a lack of MEE forcing in those simulations (and simulations by other modeling groups for CMIP5) leads to an error in determining the chemical response to external solar and geomagnetic forcing. Thus our results have great significance for any researcher analyzing the solar signal in the CMIP5 simulations.

2 Modeling and analysis methods

WACCM is a chemistry-climate general circulation model with vertical domain extending from the surface to 5.9 x 10^{-6} hPa (~140 km geometric height). The standard horizontal resolution used is 1.9° latitude by 2.5° longitude. The representation of WACCM physics in the MLT and simulations of the atmospheric response to solar and geomagnetic forcing variations are described by *Marsh et al.* [2007]. Details of recent centennial-scale coupled simulations using the current version of WACCM (version 4) and an overview of the model climate is presented by *Marsh et al.* [2013]. The chemistry module in WACCM is interactive with the dynamics through transport, radiative transfer and exothermic heating. Photochemistry associated with ion species (O^+, NO^+, O_2^+, N_2^+, N^+) is part of the standard chemistry package. For EPP, the standard model uses a lookup table parameterization for ionization-driven HO_x production, based on the work of *Solomon et al.* [1981]. For NO_x, it is assumed that 1.25 N atoms are produced per ion pair with branching ratios of 0.55/0.7 for $N(^4S)/N(^2D)$, respectively [*Porter et al.*, 1976; *Jackman et al.*, 2005].

Except for the inclusion of MEE in the EPP forcing (described in the next paragraph) the coupled model simulations presented here were set up identically to the CMIP5 simulations [for full details, see *Marsh et al.*, 2013]. We utilize the free-running dynamics version of the model (compset "B55TRWCN") that includes active ocean and sea ice components at 1° resolution. An ensemble set of three simulations was performed with all observed forcings between 1955–2005. An ensemble of three was chosen to reduce the effects from internal variability in the model in our analysis. The observed forcings include changes in surface concentrations of radiatively active species, daily solar spectral irradiance, volcanic sulfate heating, and the Quasi-Biennial Oscillation (QBO). The initial conditions for 1955 for all model components were taken from a single historical simulation (1850-2005), in an identical manner to the CMIP5 simulations. Energetic particle forcing

due to solar proton events (SPE) and auroral electron (AE) precipitation was included in the original CMIP5 simulations, hence the difference between the CMIP5 and our simulations is the addition of the new MEE forcing, as described below. The three ensemble members of simulations (49 years each) result in a total of 147 years for our analysis.

The key feature in our simulations is that we have improved the EPP forcing in WACCM by introducing 30–1000 keV radiation belt electron precipitation using the APEEP model of *van de Kamp et al.* [2016]. Note that *van de Kamp et al.* [2016] presents two versions of the MEE precipitation model depending on the geomagnetic activity index used to determine the MEE variation. Here we utilize the version driven by the *Ap* index, from now on referred to as the APEEP model for "*Ap*-driven Energetic Electron Precipitation". In the 30–1000 keV energy range, electrons provide a major ionization source at 60–90 km altitude, directly affecting mesospheric chemistry. APEEP is a proxy model, driven solely by the observed geomagnetic *Ap* index. In the model, *Ap* defines the level of magnetospheric disturbance and the location of the plasmapause, both of which are needed to calculate precipitating electron fluxes in 16 geomagnetic latitude bins between 45° and 72° for each hemisphere. The daily, zonal mean fluxes of precipitating electrons from the APEEP model were used to calculate atmospheric MEE driven ionization rates [see *van de Kamp et al.*, 2016, for details] which were then included in WACCM. The long-term ionization data sets from the APEEP model are available back to 1850 as an official part of the solar forcing recommendation for the CMIP6 simulations [*Matthes et al.*, 2017]. The same ionization data set as described by *Matthes et al.* is used here.

Figure 1 (top panel) shows the time series of monthly mean APEEP ionization in the NH at about 77 km altitude (1.7898×10^{-2} hPa). This correspond to the altitude where HO_x production in the WACCM simulations maximizes when APEEP is included. Overall, the APEEP ionization exhibits a considerable variability during all five solar cycles (SC19–SC23) with the strongest and most frequent ionization increases occurring during the declining phase of the solar cycle, in accordance with peaks in geomagnetic activity levels (not shown). In the APEEP model the electron flux characteristics are identical in the NH and SH, so that the ionization rates only have differences arising from different atmospheric conditions. The largest observed NH/SH differences are related to the longitudinal distribution of fluxes [*Andersson et al.*, 2014b], due to variations in the strength in the geomagnetic field. Those longitudinal variations are not considered when the zonal mean APEEP model is used. For the MEE energy range, these differences primarily arise

during quiet geomagnetic conditions where weak diffusive scattering processes dominate, but the magnitude of electron precipitation is very low [e.g. *Rodger et al.*, 2013, Figure 4, upper panels]. During disturbed conditions, when the magnitudes are 1-2 orders higher, strong diffusion dominates [e.g. *Horne et al.*, 2009] and no significant differences are expected with longitude or hemisphere [e.g. *Rodger et al.*, 2013, Figure 4, lower panels]. As such we expect any error in the modeling caused by using the same fluxes for NH and SH to be small compared to the overall uncertainties in the APEEP flux model.

From now on the WACCM simulations with the APEEP ionization will be referred to as "MEE_CMIP5" to highlight the addition of MEE forcing to simulations which are otherwise identical to the CMIP5 simulations. We first contrast the MEE_CMIP5 with the original CMIP5 simulations (from now on called "REF_CMIP5") and calculate the difference in HO_x, NO_x and O_3 concentrations. The purpose of this comparison is to get an overall picture of the impact that including the APEEP ionization has. We will focus this first part of the analysis on the SH, with the more detailed analysis for both hemispheres in the second part. A monthly mean analysis is made for three selected sets of years: CASE 1 includes all years (147 altogether from all three 49-year ensemble members), CASE 2 includes only the years with high APEEP ionization (36 years in total), CASE 3 includes only the years with low APEEP ionization (33 years in total). The selections are based on annual mean APEEP ionization as shown in Table 1. In the top panel of the Figure 1, red and blue indicate CASE 2 and CASE 3, respectively. The years are also listed in Table 1.

In the second part of the analysis we focus on the decadal variability due to EPP from SPE, AE, and MEE during winter (NH: December-January-February/DJF. SH: June-July-August/JJA) – this is when the EPP-driven *in situ* effects are expected to be the most pronounced. We contrast winters of high and low EPP forcing in the MEE_CMIP5 and REF_CMIP5 ensembles separately. The analysis is made for two selected sets of years: 1) high wintertime (DJF/NH and JJA/SH) APEEP ionization at 77 km altitude (51 years in the NH, 48 in the SH), and 2) low wintertime APEEP ionization at 77 km altitude (51 years in the NH, 45 in the SH), based on three-month averages of APEEP ionization. In Figure 1b (NH) and Figure 1c (SH), colors indicate the winter months of high (red) and low (blue) APEEP ionization levels. The corresponding years are also listed in Table 2.

The above selections were made with the aim to simultaneously a) contrast the extremes of the high and low APEEP ionization periods in order to identify potential responses and b) keep the number of years in the sets as large as possible to allow for robust statistical conclusions. Later, in Section 3, we will discuss how these selections affect our results. Note that although our selections are based on the APEEP ionization levels, using the geomagnetic *Ap* index (which drives both APEEP and AE in WACCM) instead would lead to very similar year groups. As an indicator of statistical robustness, we have included the 90% and 95% confidence levels in the figures. These were calculated using Student's t-test. However, as pointed out e.g. by *Ambaum* [2010], this is not a quantitative test of significance of our results: a low confidence level does not necessarily imply that the results have no physical meaning.

3 Results

3.1 MEE direct effects in the mesosphere

The monthly mean impact of the APEEP ionization on SH polar mesospheric HO_x (OH + HO_2), NO_x (NO + NO_2) and O_3 is shown in Figure 2 (VMR, volume mixing ratio) and Figure 3 (corresponding %-changes). In Figure 3, the relative difference is expressed in percents of the REF_CMIP5 VMR. Both figures show results that were averaged zonally, and over the magnetic latitudes 60–90°S. The results are shown as functions of time (month) and altitude.

For each species, the month-altitude impact patterns are similar for the three sets of years, while the magnitude of the response, and the extent of the 90% and 95% confidence regions clearly depend on the level of APEEP ionization and the number of years included in the sets. As expected, these confidence regions are most extended for CASE 1, which includes the largest number of years. For all the species, the magnitude of the response is largest for the high APEEP ionization years (CASE 2) and smallest for the low APEEP ionization years (CASE 3), as expected. In CASE 3, there is a clearly different NO_x response above 80 km during the summer months (Figure 2, mid-right panel). However, this response is in the region of lesser statistical robustness and thus could be caused by background variability.

For the high APEEP ionization years (CASE 2), HO_x enhancements of up to 0.6 ppbv (increase of 20% from REF_CMIP5) are seen during May–July at altitudes between 65

and 85 km. When considering CASE 1 (all years) and CASE 3 (low APEEP ionization years), the VMR response is smaller than for CASE 2 but the magnitude of the changes produced still exceeds 10%. Outside of these months, the HO_x increases between 60 and 90 km, where the largest concentrations of HO_x are observed in general, are very small. At altitudes <60 km and >90 km, where the HO_x background is very small, MEE results in a small reduction. Note that above 90 km there would be an HO_x increase, rather than decrease, if we also included atomic hydrogen in HO_x (not shown). Thus, the decrease seen in our plots at these altitudes indicates a change in HO_x partitioning towards H, caused by the extra production of atomic oxygen by MEE and reactions such as O + OH $\rightarrow$ O_2 + H.

For NO_x, the APEEP-driven VMR increase peaks at 80–100 km, where it is seen throughout all seasons. This is consistent with the APEEP ionization typically peaking around 90 km [*van de Kamp et al.*, 2016]. For the years of high APEEP ionization (CASE 2), the VMR response reaches 200 ppbv in June–July and is smallest in December–January (20-50 ppbv). At lower altitudes, there is a clear seasonal cycle with a 20-30 % increase down to stratopause level **focused on** winter months when NO_x is descending inside the polar vortex. Above 100 km, NO_x decreases but relatively this effect is very small and not statistically significant. These effects are similar for the other sets of years, albeit smaller in magnitude especially for low APEEP ionization (CASE 3).

As seen in Figure 3, the NO_x percentage response patterns are quite different from those of VMR shown in Figure 2. The relative increase is largest during the summer due to the lower natural NO_x background values, exceeding 200% for CASE 2. During mid-winter, when NO_x is already enhanced due to AE and descent, the APEEP ionization leads to an increase of over 20% in the average mesospheric NO_x.

For O_3, the VMR response pattern below 85 km is similar to that of HO_x inverted (so that high HO_x correlates with low O_3), but shifted to lower altitudes and covering a wider range of altitudes. From March to September, ozone decreases at 60–80 km by up to 0.2–0.3 ppmv depending on the CASE, with strongest and most extended response seen for years of high APEEP ionization (CASE 2). Around its secondary maximum (at 90–100 km), ozone has a response which during spring and autumn months reaches magnitudes similar to those seen at lower altitudes. However, in the context of total O_x (O + O_3) the magnitude of the effect is small because at these altitudes atomic oxygen concen-

tration is several orders of magnitude larger than that of ozone. In fact, if we plotted O_x instead of ozone, we would see an increase rather than a decrease at the secondary maximum. This is caused by extra atomic oxygen production by MEE. Thus the decrease seen in ozone indicates a change in the O_x partitioning towards O. In percentage, the mesospheric O_3 response is seen during all but the mid summer months and it is strongest in spring and autumn periods, varying between 10% and 30% in February–October in CASE 2. The equinox pattern does not coincide with the HO_x increase, indicating that the NO_x enhancements could have an additional effect on HO_x partitioning and ozone depletion [*Verronen and Lehmann*, 2015] and could modulate the formation of the tertiary ozone maximum [*Sofieva et al.*, 2009]. On the other hand, during mid winter the polar night covers a larger area over the polar cap. Thus the effect of ozone-depleting catalytic cycles, which depend on solar illumination, should be diminished leading to a smaller MEE response. The percentage difference is also affected by the background amount of ozone which is generally higher during winter and results in a smaller relative response.

Although not shown, the magnitude of the NH response of mesospheric HO_x and ozone is very similar to that presented for the SH. For NO_x, the maximum wintertime enhancement is somewhat smaller and less pronounced than in the SH, which corresponds to larger dynamical variability in the NH, including the more frequent occurrence of Sudden Stratospheric Warming events [*Päivärinta et al.*, 2013]. For all the species, the month-altitude response patterns in the NH are very similar to those in the SH, except that the maximum percentage change in ozone peaks in the mid winter instead of the autumn months, possibly an indication of the earlier formation of the polar vortex in the SH.

3.2 MEE indirect effects in the stratosphere

Figure 4 shows the monthly mean APEEP impact on NO_x and O_3 in the SH polar stratosphere and lower mesosphere (15–65 km) as %-change (like Figure 3, but lower altitude range). The electron energy range used in the APEEP ionization model provides direct forcing only at altitudes above 60 km, so the stratospheric response is entirely due to a) transport of APEEP-NO_x from above, b) chemical-dynamical coupling, or c) combination of a and b. A tongue-like structure of excess APEEP-NO_x descends from the lower mesosphere starting in autumn, causing an ozone decrease in the stratosphere. The magnitude of the response is largest for the years of high APEEP ionization (CASE 2) and smallest for the low APEEP years (CASE 3). Because there is no direct MEE effect in the

stratosphere, the early winter increase around 30 km must be related to descending NO_x, some of which remains over the summer months. Note that a similar early winter EPP effect also appears to be present in NO_x experimental observations [*Funke et al.*, 2014a, Figure 9].

The descending APEEP-NO_x reaches altitudes as low as 30 km by November with the maximum increase being 10–20% depending on the CASE. Corresponding ozone decreases of 5–8% are seen at altitudes between 30–50 km in all CASES. For CASE 1 and 2, part of the stratospheric ozone response (a decrease) is within the 90-95 % significance region. In CASE 3, none of the ozone response below 50 km is statistically robust, which may indicate a larger variation in percentages for CASE 3, probably due to the lower average background ionization in this case. Nevertheless, stratospheric NO_x and ozone are affected in years of low APEEP ionization even though the direct APEEP forcing is restricted to altitudes above 60 km. Above 55 km, the direct effect of the ozone response (see previous section) is influenced by both HO_x and NO_x increases.

To consider the robustness of the ozone response in the middle atmosphere, Figure 5 shows a statistical analysis of the wintertime APEEP impact on ozone, both in VMR and percentages, as a function of altitude. The responses were averaged over SH polar latitudes of 60–90°, and over the months of June to August in the ensembles. The month selection covers the period of strongest, most robust ozone response in the stratosphere (as seen in Figure 4). The graphs also include the standard error of the mean (SEM) of the difference, calculated as

$$SEM = \sqrt{\frac{STD_1^2 + STD_2^2}{n}} \tag{1}$$

where STD_1 and STD_2 are yearly standard deviations of the MEE_CMIP5 and REF_CMIP5 simulations, respectively, and n is the number of years.

At mesospheric altitudes, ozone loss is connected directly to APEEP ionization and the resulting HO_x increase, and this response is generally very robust. This is demonstrated through the SEM being clearly smaller than the magnitude of the response. In the stratosphere, the decrease in ozone is caused by the descent of APEEP-NO_x and is strongly affected by dynamical variability. At 30–50 km, the SEM becomes comparable to the magnitude of the response. The SEM increases with decreasing number of included years, thus the ozone response is clearly most robust for CASE 1 which includes all years.

For years of high and low APEEP ionization, the response exceeds the SEM above 40 km and at 30–40 km, respectively.

3.3 Decadal variability due to EPP in mesosphere and stratosphere

In this section, we will investigate the variability of HO_x, NO_x, and ozone by analyzing the differences between the responses for high and low EPP ionization winters as listed in Table 2. Figures 6 and 7 present the wintertime HO_x and ozone variability at altitudes between 70 and 80 km for the NH and the SH, respectively.

Results from MEE_CMIP5 (panels a and c) show clear differences between high EPP and low EPP winters in both hemispheres. At geomagnetic latitudes directly affected by radiation belt electrons (55–72°), there is up to 15% more HO_x in high EPP winters (panel a). The zonal asymmetry seen in the HO_x distribution is caused by different illumination conditions over the affected geomagnetic latitudes, i.e. at lower geographic latitudes the higher level of solar-driven water vapor photodissociation leads to higher amounts of background HO_x and smaller EPP response in relative terms. The strongest ozone variation coincides with the largest HO_x variation, with ozone decreases of about 8% in the NH and 10% in the SH.

On the other hand, the results from REF_CMIP5 (panels b and d), which does not include direct APEEP ionization in the mesosphere, are clearly different. Here, the NH HO_x and ozone generally lack a clear correlation pattern. In the SH in the REF_CMIP5, around 10% increase in HO_x is seen at high geomagnetic latitudes, higher than the outer radiation belt latitudes (panel 7b), during high EPP winters. This is likely caused by a combination of production due to SPEs and changes in HO_x partitioning due to increased NO_x [*Verronen and Lehmann*, 2015]. In this case the corresponding ozone decrease is less than 5% and is outside of the 90% confidence limit (panel 7d).

Figures 8 and 9 present the NO_x and ozone variability (%) in the stratosphere–lower mesosphere at high polar latitudes in the NH (≥70°) and SH (≥60°), respectively. In the NH, a smaller latitude range was used because the area of the polar vortex (which we wanted to cover in wintertime) is typically smaller there than in the SH. Note, however, that the results for 70–90°N (shown in Figure 8) are very similar to those for 60–90°N (not shown). Both Figures 8 and 9 display the full 12 month progression, with winter months placed in the middle of the x-axis to ease comparison.

In the NH (Figure 8) the dynamical variability is much stronger than in the SH and includes sudden stratospheric warmings [*Päivärinta et al.*, 2013]. As a result the response to MEE is less pronounced than in the SH (Figure 9) [*Funke et al.*, 2014a,b]. Although individual winters may show strong NO_x descent, the signal becomes less clear when averaged over decadal time scales, even when APEEP ionization is included. As a result of the dominating dynamical variability in the NH the timing of the descent can also vary from year-to-year much more than in the SH, which easily leads to smearing of the signal when averaging. We note that the early winter NO_x enhancement signal in both experiments is due to the so-called Halloween SPEs in 2003.

In the SH (Figure 9), the NO_x difference between high and low EPP winters is clear in both MEE_CMIP5 and REF_CMIP5 simulations. The difference shows a pattern of descending NO_x from early winter (April) to early summer (December) with and without the APEEP ionization. The inclusion of the APEEP ionization significantly adds to this NO_x variability - the highest variability goes from 50% to 70%. For the MEE_CMIP5 results in Figure 9a, the NO_x increase during High EPP forcing at 30–50 km is between 40–70%. The corresponding REF_CMIP5 signature (Figure 9b), which is due to the descent of AE-produced NO_x, is between 30% and 50%.

Stratospheric ozone loss coincides with the NO_x descent in both Figures 9c and 9d. During high EPP and from early winter (April) to early summer (December), there is up to 7% and 2% less ozone at 25–50 km with and without APEEP, respectively. Although the response patterns are similar, in the MEE_CMIP5 results the effect is much stronger and statistically significant. As a clear pattern in both simulations, the ozone depletion persists throughout the summer, descending in altitude and decreasing in magnitude with time, with final remnants seen until early next winter at about 25 km. The fact that the late summer signal seems to be more robust in the REF_CMIP5 simulation could be simply caused by internal model variability. The increase of ozone peaking at about 30 km in August-October, is caused by the enhanced NO_x converting active chlorine and bromine to their reservoir species, which leads to less ozone loss by catalytic reactions [*Jackman et al.*, 2009].

When considering the difference between high and low EPP years in the MEE_CMIP5 simulation, in the mesosphere the HO_x and ozone signal is strong and only weakly dependent on the number of years included in the analysis (not shown). By using stricter selec-

tion criteria, leading to a smaller number of winters with larger differences in EPP forcing, the HO_x and ozone response gets consistently stronger for the latitudes affected by outer radiation belt electrons. However, this is not the case when considering the stratospheric difference. The selection criteria are much more a critical issue, e.g., as reducing the number of years results in an ozone response which is not necessarily stronger but quickly becomes statistically less robust (i.e. does not reach the 95% confidence level). For example, this happens in the SH when the total number of years is reduced from 50 to about 30. This indicates that a time series of considerable length, extending over several decades, is needed to robustly identify the signal.

In our analysis, we are implicitly assuming the 147 individual years as samples of the same population. If the response is not invariant over the timeseries, it would add to the variance and lead to an underestimate of the statistical significance of the response to MEE and EPP in general. And if there are any large trends, we could be overestimating the background variability, which would in fact make the response harder to detect. The fact that we still see a statistically significant response implies that the signal is probably stronger and more robust rather than the other way around. It also shows that the signal could be detectable in a real, observational timeseries rather than in an idealized constant forcing scenario, for example.

4 Discussion

Our results can be compared to previous studies although it should be carefully noted that these typically consider only a portion of our 147-year (3×49 year ensemble) time series due to, e.g., limited availability of experimental data and/or forcing data for atmospheric simulations. Overall, there is a qualitative agreement with previous simulation studies and satellite-based observations which suggested a clear EPP-driven impact and an important role for MEE in the polar middle atmosphere.

Our results on the APEEP ionization impact on mesospheric HO_x and O_3 are in very good agreement with satellite observations. The magnitude of our simulated HO_x responses (0.3–0.6 ppmv) as well as their spatial distributions are similar to the results based on satellite data analysis [*Andersson et al.*, 2014b; *Zawedde et al.*, 2016]. Also the magnitude of our simulated mesospheric ozone variability over decadal time scales agrees well with observations [*Andersson et al.*, 2014a]. This seems to indicate that the level of

the APEEP forcing, which directly affects the mesosphere in our simulations, is reasonable – at least in the middle and upper mesosphere where the APEEP ionization peaks.

In the SH upper stratosphere we found an EPP-driven decadal variability of up to 70% in NO_x and up to 7% in ozone. The magnitude of the ozone response is within but at lower end of the 5–15% range of response obtained from satellite data analysis [*Fytterer et al.*, 2015; *Damiani et al.*, 2016] and the 3–20% range from previous simulations [*Baumgaertner et al.*, 2011; *Semeniuk et al.*, 2011; *Rozanov et al.*, 2012]. Compared to previous work our study uses fully time-dependent EPP forcing and provides the longest analyzed time series so far, extending almost five solar cycles, giving us better statistical robustness and allowing for more general conclusions.

The MEE ionization, which directly affects the polar mesosphere, has been a major source of uncertainty in the EPP forcing used in earlier simulations. As our results now indicate, simulations using the APEEP model generally agree better with the observed ozone response, in both the mesosphere and the stratosphere. As the comparison to the earlier CMIP5 simulations (without MEE) shows, the decadal polar ozone response depends very much on MEE, and any analysis based on those CMIP5 simulations will significantly underestimate the EPP signal. In the forthcoming CMIP6 simulations, it is likely that the situation will drastically improve as the APEEP model is part of the official solar forcing recommendation.

The amount of the descending EPP-NO_x is clearly important for the magnitude of the stratospheric ozone response. In WACCM, underestimation of polar mesospheric NO_x has been reported, likely caused by some combination of missing *in-situ* production by EPP and also weak transport of NO_x from the lower thermosphere [*Randall et al.*, 2015]. Further model development is needed to better simulate dynamically perturbed winters and improve the mesosphere-to-stratosphere descent in high-top models such as WACCM [*Funke et al.*, 2017]. MEE is included in our simulations through the APEEP model. This work is therefore a significant contribution towards understanding the importance of the missing MEE. It is likely that the production and transport of lower thermospheric NO_x is the primary remaining issue leading to any NO_x underestimation. It should be noted that in the WACCM simulations of *Randall et al.* [2015] and *Funke et al.* [2017] the model dynamics were nudged to the MERRA reanalysis data, and these studies considered just two individual, highly-disturbed NH winters. Therefore, as we are using WACCM with

free-running dynamics and consider a time series of 147 years for both hemispheres, those previously reported NO_x issues should not be critically affecting our results. Additional adjustment of EPP-NO_x may also be achieved by including the lower ionospheric (D-region) chemistry which is shown to increase the production in the mesosphere [*Andersson et al.*, 2016]. One might also consider the inclusion of relativistic electron precipitation (>1 MeV) which would be expected to directly impact stratopause altitudes. Finally, enhanced eddy diffusion in the mesosphere-lower thermosphere region would increase the transport of auroral NO_x into the mesosphere and below, which seems to yield better agreement with observations [*Meraner and Schmidt*, 2016][*Matthes et al.*, 2017, Figure 13].

5 Conclusions

Here we have introduced long-term MEE forcing to the Whole Atmosphere Community Climate Model (CESM/WACCM). We simulated EPP-driven variability, including the new MEE forcing, in polar ozone over a period of 147 years (3-member ensemble of 49-year simulations). The results were compared with those from the CMIP5 climate simulations in order to study the contribution of the additional MEE forcing. The main results can be summarized as follows.

- EPP-driven variability in mesospheric HO_x and ozone is clear in both hemispheres: the ozone difference between high and low EPP winters varies from 8% to 10% at 70–80 km (less ozone when EPP is high).
- Stratospheric ozone response is distinct in the SH: EPP-driven ozone variability of 2-7% is seen down to about 25–35 km.
- The contribution of MEE is very important to the total EPP-driven response. In the mesosphere, there is either a a small or no clear response in HO_x and ozone without the inclusion of direct ionization by MEE. In the stratosphere, inclusion of MEE enhances the response in NO_x and ozone by a factor of about two.
- Our study indicates that in order to assess the indirect EPP effect in the stratosphere in a robust way, multi-decadal simulations are needed to overcome the levels of dynamical variability in the model.

Acknowledgments

The work of M.E.A., P.T.V., A.S., S.-M.P., N.K. and M.v.d.K. was supported by the Academy of Finland through the projects #276926 (SECTIC: Sun-Earth Connection Through Ion Chemistry), #258165, and #265005 (CLASP: Climate and Solar Particle Forcing). D.R.M. was supported in part by NASA grant NNX12AD04G. M.A.C. was supported by the Natural Environment Research Council. The National Center for Atmospheric Research is operated by the University Corporation for Atmospheric Research under sponsorship of the National Science Foundation. All model data used are available from the corresponding author by request. CESM source code is distributed through a public subversion repository (http://www.cesm.ucar.edu/models/cesm1.0/).

References

Ambaum, M. H. P. (2010), Significance tests in climate science, *J. Climate*, *23*(22), 5927–5932, doi:10.1175/2010JCLI3746.1.

Andersson, M. E., P. T. Verronen, S. Wang, C. J. Rodger, M. A. Clilverd, and B. Carson (2012), Precipitating radiation belt electrons and enhancements of mesospheric hydroxyl during 2004-2009, *J. Geophys. Res.*, *117*, D09,304, doi:10.1029/2011JD017246.

Andersson, M. E., P. T. Verronen, C. J. Rodger, M. A. Clilverd, and A. Seppälä (2014a), Missing driver in the Sun-Earth connection from energetic electron precipitation impacts mesospheric ozone, *Nature Commun.*, *5*(5197), doi:10.1038/ncomms6197.

Andersson, M. E., P. T. Verronen, C. J. Rodger, M. A. Clilverd, and S. Wang (2014b), Longitudinal hotspots in the mesospheric OH variations due to energetic electron precipitation, *Atmos. Chem. Phys.*, *14*, 1095–1105, doi:10.5194/acp-14-1095-2014.

Andersson, M. E., P. T. Verronen, D. R. Marsh, S.-M. Päivärinta, and J. M. C. Plane (2016), WACCM-D – Improved modeling of nitric acid and active chlorine during energetic particle precipitation, *J. Geophys. Res. (Atmos.)*, *121*, 10,328–10,341, doi:10.1002/2015JD024173.

Arsenovic, P., E. Rozanov, A. Stenke, B. Funke, J. M. Wissing, K. Mursula, F. Tummon, and T. Peter (2016), The influence of middle range energy electrons on atmospheric chemistry and regional climate, *J. Atmos. Sol.-Terr. Phys.*, doi:10.1016/j.jastp.2016.04.008.

Baumgaertner, A. J. G., A. Seppälä, P. Jöckel, and M. A. Clilverd (2011), Geomagnetic activity related NO_x enhancements and polar surface air temperature variability in

a chemistry climate model: modulation of the NAM index, *Atmos. Chem. Phys.*, *11*, 4521–4531, doi:10.5194/acp-11-4521-2011.

Callis, L. B., and J. D. Lambeth (1998), NO_y formed by precipitating electron events in 1991 and 1992: Descent into the stratosphere as observed by ISAMS, *Geophys. Res. Lett.*, *25*, 1875–1878, doi:10.1029/98GL01219.

Codrescu, M. V., T. J. Fuller-Rowell, R. G. Roble, and D. S. Evans (1997), Medium energy particle precipitation influences on the mesosphere and lower thermosphere, *J. Geophys. Res.*, *102*, 19,977–19,988.

Damiani, A., B. Funke, M. L. Santee, R. R. Cordero, and S. Watanabe (2016), Energetic particle precipitation: A major driver of the ozone budget in the Antarctic upper stratosphere, *Geophys. Res. Lett.*, *43*, 3554–3562, doi:10.1002/2016GL068279.

Funke, B., A. Baumgaertner, M. Calisto, T. Egorova, C. H. Jackman, J. Kieser, A. Krivolutsky, M. López-Puertas, D. R. Marsh, T. Reddmann, E. Rozanov, S.-M. Salmi, M. Sinnhuber, G. P. Stiller, P. T. Verronen, S. Versick, T. von Clarmann, T. Y. Vyushkova, N. Wieters, and J. M. Wissing (2011), Composition changes after the "Halloween" solar proton event: the High-Energy Particle Precipitation in the Atmosphere (HEPPA) model versus MIPAS data intercomparison study, *Atmos. Chem. Phys.*, *11*, 9089–9139, doi:10.5194/acp-11-9089-2011.

Funke, B., M. López-Puertas, G. P. Stiller, and T. von Clarmann (2014a), Mesospheric and stratospheric NO_y produced by energetic particle precipitation during 2002–2012, *J. Geophys. Res.*, *119*, 4429–4446, doi:10.1002/2013JD021404.

Funke, B., M. López-Puertas, L. Holt, C. E. Randall, G. P. Stiller, and T. von Clarmann (2014b), Hemispheric distributions and interannual variability of NO_y produced by energetic particle precipitation in 2002–2012, *J. Geophys. Res.*, *119*, 13,565–13,582, doi:10.1002/2014JD022423.

Funke, B., W. Ball, S. Bender, A. Gardini, V. L. Harvey, A. Lambert, M. López-Puertas, D. R. Marsh, K. Meraner, H. Nieder, S.-M. Päivärinta, K. Pérot, C. E. Randall, T. Reddmann, E. Rozanov, H. Schmidt, A. Seppälä, M. Sinnhuber, T. Sukhodolov, G. P. Stiller, N. D. Tsvetkova, P. T. Verronen, S. Versick, T. von Clarmann, K. A. Walker, and V. Yushkov (2017), HEPPA-II model-measurement intercomparison project: EPP indirect effects during the dynamically perturbed NH winter 2008–2009, *Atmos. Chem. Phys.*, *17*, 3573–3604, doi:10.5194/acp-17-3573-2017.

Fytterer, T., M. G. Mlynczak, H. Nieder, K. Pérot, M. Sinnhuber, G. Stiller, and J. Urban (2015), Energetic particle induced intra-seasonal variability of ozone inside the Antarctic polar vortex observed in satellite data, *Atmos. Chem. Phys.*, *15*(6), 3327–3338, doi: 10.5194/acp-15-3327-2015.

Gray, L. J., J. Beer, M. Geller, J. D. Haigh, M. Lockwood, K. Matthes, U. Cubasch, D. Fleitmann, G. Harrison, L. Hood, J. Luterbacher, G. A. Meehl, D. Shindell, B. van Geel, and W. White1 (2010), Solar influences on climate, *Rev. Geophys.*, *48*, RG4001, doi:10.1029/2009RG000282.

Horne, R. B., M. M. Lam, and J. C. Green (2009), Energetic electron precipitation from the outer radiation belt during geomagnetic storms, *Geophys. Res. Lett.*, *36*, L19,104, doi:10.1029/2009GL040236.

Jackman, C. H., R. D. McPeters, G. J. Labow, E. L. Fleming, C. J. Praderas, and J. M. Russel (2001), Northern hemisphere atmospheric effects due to the July 2000 solar proton events, *Geophys. Res. Lett.*, *28*, 2883–2886.

Jackman, C. H., M. T. DeLand, G. J. Labow, E. L. Fleming, D. K. Weisenstein, M. K. W. Ko, M. Sinnhuber, and J. M. Russell (2005), Neutral atmospheric influences of the solar proton events in October-November 2003, *J. Geophys. Res.*, *110*, A09S27, doi: 10.1029/2004JA010888.

Jackman, C. H., D. R. Marsh, F. M. Vitt, R. R. Garcia, E. L. Fleming, G. J. Labow, C. E. Randall, M. López-Puertas, B. Funke, T. von Clarmann, and G. P. Stiller (2008), Short- and medium-term atmospheric constituent effects of very large solar proton events, *Atmos. Chem. Phys.*, *8*, 765–785, doi:10.5194/acp-8-765-2008.

Jackman, C. H., D. R. Marsh, F. M. Vitt, R. R. Garcia, C. E. Randall, E. L. Fleming, and S. M. Frith (2009), Long-term middle atmospheric influence of very large solar proton events, *J. Geophys. Res.*, *114*, D11,304, doi:10.1029/2008JD011415.

Langematz, U., J. L. Grenfell, K. Matthes, P. M. nad M. Kunze, B. Steil, and C. Brühl (2005), Chemical effects in 11-year solar cycle simulations with the Freie Universität Berlin Climate Middle Atmosphere Model with online chemistry (FUB-CMAM-CHEM), *Geophys. Res. Lett.*, *32*, L13,803, doi:10.1029/2005GL022686.

Lu, H., M. A. Clilverd, A. Seppälä, and L. L. Hood (2008), Geomagnetic perturbations on stratospheric circulation in late winter and spring, *J. Geophys. Res.*, *113*, D16,106, doi:10.1029/2007JD008915.

584 Marsh, D. R., R. R. Garcia, D. E. Kinnison, B. A. Boville, F. Sassi, S. C. Solomon, and
585 K. Matthes (2007), Modeling the whole atmosphere response to solar cycle changes in
586 radiative and geomagnetic forcing, *J. Geophys. Res. (Atmos.)*, *112*(D11), D23,306, doi:
587 10.1029/2006JD008306.

588 Marsh, D. R., M. Mills, D. Kinnison, J.-F. Lamarque, N. Calvo, and L. Polvani (2013),
589 Climate change from 1850 to 2005 simulated in CESM1(WACCM), *J. Climate*, *26*(19),
590 7372–7391, doi:10.1175/JCLI-D-12-00558.1.

591 Matthes, K., B. Funke, M. E. Andersson, L. Barnard, J. Beer, P. Charbonneau, M. A. Clil-
592 verd, T. Dudok de Wit, M. Haberreiter, A. Hendry, C. H. Jackman, M. Kretschmar,
593 T. Kruschke, M. Kunze, U. Langematz, D. R. Marsh, A. Maycock, S. Misios,
594 C. J. Rodger, A. A. Scaife, A. Seppälä, M. Shangguan, M. Sinnhuber, K. Tourpali,
595 I. Usoskin, M. van de Kamp, P. T. Verronen, and S. Versick (2017), Solar forcing for
596 CMIP6, *Geosci. Model Dev.*, *10*, 2247–2302, doi:10.5194/gmd-10-2247-2017.

597 Meraner, K., and H. Schmidt (2016), Transport of nitrogen oxides through the
598 winter mesopause in HAMMONIA, *J. Geophys. Res.*, *121*(6), 2556–2570, doi:
599 10.1002/2015JD024136.

600 Päivärinta, S.-M., A. Seppälä, M. E. Andersson, P. T. Verronen, L. Thölix, and E. Kyrölä
601 (2013), Observed effects of solar proton events and sudden stratospheric warmings on
602 odd nitrogen and ozone in the polar middle atmosphere, *J. Geophys. Res. (Atmos.)*, *118*,
603 6837–6848, doi:10.1002/jgrd.50486.

604 Porter, H. S., C. H. Jackman, and A. E. S. Green (1976), Efficiencies for production of
605 atomic nitrogen and oxygen by relativistic proton impact in air, *J. Chem. Phys.*, *65*,
606 154–167.

607 Randall, C. E., D. W. Rusch, R. M. Bevilacqua, K. W. Hoppel, and J. D. Lumpe (1998),
608 Polar Ozone and Aerosol Measurement (POAM) II stratospheric NO_2, 1993–1996, *J.*
609 *Geophys. Res. (Atmos.)*, *103*(D21), 28,361–28,371, doi:10.1029/98JD02092.

610 Randall, C. E., V. L. Harvey, G. L. Manney, Y. Orsolini, M. Codrescu, C. Sioris, S. Bro-
611 hede, C. S. Haley, L. L. Gordley, J. M. Zawodny, and J. M. Russell (2005), Strato-
612 spheric effects of energetic particle precipitation in 2003-2004, *Geophys. Res. Lett.*, *32*,
613 L05,802, doi:10.1029/2004GL022003.

614 Randall, C. E., V. L. Harvey, D. E. Siskind, J. France, P. F. Bernath, C. D. Boone, and
615 K. A. Walker (2009), NO_x descent in the Arctic middle atmosphere in early 2009, *Geo-*
616 *phys. Res. Lett.*, *36*, L18,811, doi:10.1029/2009GL039706.

Randall, C. E., V. L. Harvey, L. A. Holt, D. R. Marsh, D. Kinnison, B. Funke, and P. F. Bernath (2015), Simulation of energetic particle precipitation effects during the 2003–2004 Arctic winter, *J. Geophys. Res. (Space Phys.)*, *120*, 5035–5048, doi: 10.1002/2015JA021196.

Rodger, C. J., M. A. Clilverd, J. C. Green, and M. M. Lam (2010a), Use of POES SEM-2 observations to examine radiation belt dynamics and energetic electron precipitation into the atmosphere, *J. Geophys. Res. (Space Phys.)*, *115*, A04,202, doi: 10.1029/2008JA014023.

Rodger, C. J., A. J. Kavanagh, M. A. Clilverd, and S. R. Marple (2013), Comparison between POES energetic electron precipitation observations and riometer absorptions: Implications for determining true precipitation fluxes, *J. Geophys. Res. (Space Phys.)*, *118*, 7810–7821, doi:10.1002/2013JA019439.

Rozanov, E., L. Callis, M. Schlesinger, F. Yang, N. Andronova, and V. Zubov (2005), Atmospheric response to NO_y source due to energetic electron precipitation, *Geophys. Res. Lett.*, *32*, L14,811, doi:10.1029/2005GL023041.

Rozanov, E., M. Calisto, T. Egorova, T. Peter, and W. Schmutz (2012), The influence of precipitating energetic particles on atmospheric chemistry and climate, *Surveys in Geophys.*, *33*, 483–501, doi:10.1007/s10712-012-9192-0.

Semeniuk, K., V. I. Fomichev, J. C. McConnell, C. Fu, S. M. L. Melo, and I. G. Usoskin (2011), Middle atmosphere response to the solar cycle in irradiance and ionizing particle precipitation, *Atmos. Chem. Phys.*, *11*, 5045–5077, doi:10.5194/acp-11-5045-2011.

Seppälä, A., and M. A. Clilverd (2014), Energetic particle forcing of the northern hemisphere winter stratosphere: Comparison to solar irradiance forcing., *Front. Physics*, *2:25*, doi:10.3389/fphy.2014.00025.

Seppälä, A., P. T. Verronen, M. A. Clilverd, C. E. Randall, J. Tamminen, V. F. Sofieva, L. Backman, and E. Kyrölä (2007), Arctic and Antarctic polar winter NO_x and energetic particle precipitation in 2002–2006, *Geophys. Res. Lett.*, *34*, L12,810, doi: 10.1029/2007GL029733.

Seppälä, A., C. E. Randall, M. A. Clilverd, E. Rozanov, and C. J. Rodger (2009), Geomagnetic activity and polar surface air temperature variability, *J. Geophys. Res.*, *114*, A10,312, doi:10.1029/2008JA014029.

Seppälä, A., H. Lu, M. A. Clilverd, , and C. J. Rodger (2013), Geomagnetic activity signatures in wintertime stratosphere wind, temperature, and wave response, *J. Geophys.*

Res., *118*, 2169–2183, doi:10.1002/jgrd.50236.

Seppälä, A., K. Matthes, C. E. Randall, and I. A. Mironova (2014), What is the solar influence on climate? Overview of activities during CAWSES-II, *Prog. Earth Planet. Sci.*, *1:24*, doi:10.1186/s40645-014-0024-3.

Sinnhuber, B.-M., P. von der Gathen, M. Sinnhuber, M. Rex, G. König-Langlo, and S. J. Oltmans (2006), Large decadal scale changes of polar ozone suggest solar influence, *Atmos. Chem. Phys.*, *6*, 1835–1841.

Siskind, D. E., G. E. Nedoluha, C. E. Randall, M. Fromm, and J. M. Russell III (2000), An assessment of Southern Hemisphere stratospheric NO_x enhancements due to transport from the upper atmosphere, *Geophys. Res. Lett.*, *27*(3), 329–332.

Sofieva, V. F., E. Kyrölä, P. T. Verronen, A. Seppälä, J. Tamminen, D. R. Marsh, A. K. Smith, J.-L. Bertaux, A. Hauchecorne, F. Dalaudier, D. Fussen, F. Vanhellemont, O. Fanton d'Andon, G. Barrot, M. Guirlet, T. Fehr, and L. Saavedra (2009), Spatio-temporal observations of the tertiary ozone maximum, *Atmos. Chem. Phys.*, *9*, 4439–4445, doi:10.5194/acp-9-4439-2009.

Solomon, S., D. W. Rusch, J.-C. Gérard, G. C. Reid, and P. J. Crutzen (1981), The effect of particle precipitation events on the neutral and ion chemistry of the middle atmosphere: II. Odd hydrogen, *Planet. Space Sci.*, *8*, 885–893.

van de Kamp, M., A. Seppälä, M. A. Clilverd, C. J. Rodger, P. T. Verronen, and I. C. Whittaker (2016), A model providing long-term datasets of energetic electron precipitation during geomagnetic storms, *J. Geophys. Res. (Atmos.)*, *121*, 12,520–12,540, doi:10.1002/2015JD024212.

Verronen, P. T., and R. Lehmann (2015), Enhancement of odd nitrogen modifies mesospheric ozone chemistry during polar winter, *Geophys. Res. Lett.*, *42*, 10,445–10,452, doi:10.1002/2015GL066703.

Verronen, P. T., A. Seppälä, E. Kyrölä, J. Tamminen, H. M. Pickett, and E. Turunen (2006), Production of odd hydrogen in the mesosphere during the January 2005 solar proton event, *Geophys. Res. Lett.*, *33*, L24,811, doi:10.1029/2006GL028115.

Verronen, P. T., C. J. Rodger, M. A. Clilverd, and S. Wang (2011), First evidence of mesospheric hydroxyl response to electron precipitation from the radiation belts, *J. Geophys. Res.*, *116*, D07,307, doi:10.1029/2010JD014965.

Verronen, P. T., M. E. Andersson, C. J. Rodger, M. A. Clilverd, S. Wang, and E. Turunen (2013), Comparison of modeled and observed effects of radiation belt electron precip-

683 itation on mesospheric hydroxyl and ozone, *J. Geophys. Res.*, *118*, 11,419–11,428, doi:
684 10.1002/jgrd.50845.
685 Zawedde, A. E., H. N. Tyssøy, R. Hibbins, P. J. Espy, L.-K. G. Ødegaard, M. I. Sandan-
686 ger, and J. Stadsnes (2016), The impact of energetic electron precipitation on meso-
687 spheric hydroxyl during a year of solar minimum, *J. Geophys. Res. (Space Phys.)*, *121*,
688 5914–5929, doi:10.1002/2016JA022371.

689 **Table 1.** Selected sets of years for the analysis of the impact due to the APEEP ionization. The selection cri-
690 teria for CASE 2 and 3 **are** based on the annual mean ionization rate at ≈77 km altitude (1.7898×10^{-2} hPa).
691 This produces two groups of years that are roughly the same size but have a clear separation in average ioniza-
692 tion rate levels.

Set	Ionization rate selection criteria [ion pairs $cm^{-3}s^{-1}$@77km]	Years	# years
CASE 1	–	All years: 1957-2005	147
CASE 2	annual mean > 75	1957-60, 1974, 1982-84, 1989, 1991, 1994, 2003	36
CASE 3	annual mean < 40	1964-66, 1969-71, 1980, 1987, 1996-98	33

693 **Table 2.** Selected sets of high and low EPP years for the analysis of EPP-driven variability in mesosphere
694 and stratosphere. The selection limits are set at the median of the APEEP ionization at ≈77 km altitude
695 (1.7898×10^{-2} hPa) over winter season ±10 ion pairs/cm^3/s, separately for the two hemispheres. For the NH,
696 the years listed correspond to the year of the December e.g. DJF 1974 = December 1974 – February 1975.
697 The number of years is the total from all ensemble members, i.e. three times the number of years listed.

Set	Ionization rate selection criteria [ion pairs $cm^{-3}s^{-1}$@77km]	Years	# years
High NH	DJF > 55	1957-60, 1972, 1974, 1981-82, 1984-85, 1988-89, 1991-93, 2003, 2004	51
High SH	JJA > 50	1957-61, 1974, 1978, 1981-84, 1989-91, 2000, 2003	48
Low NH	DJF < 35	1961, 1964-65, 1968-71, 1976, 1979, 1986, 1990, 1995-98, 2000-01	51
Low SH	JJA < 30	1964-67, 1969, 1971, 1976, 1986-88, 1995-97, 2001-02	45

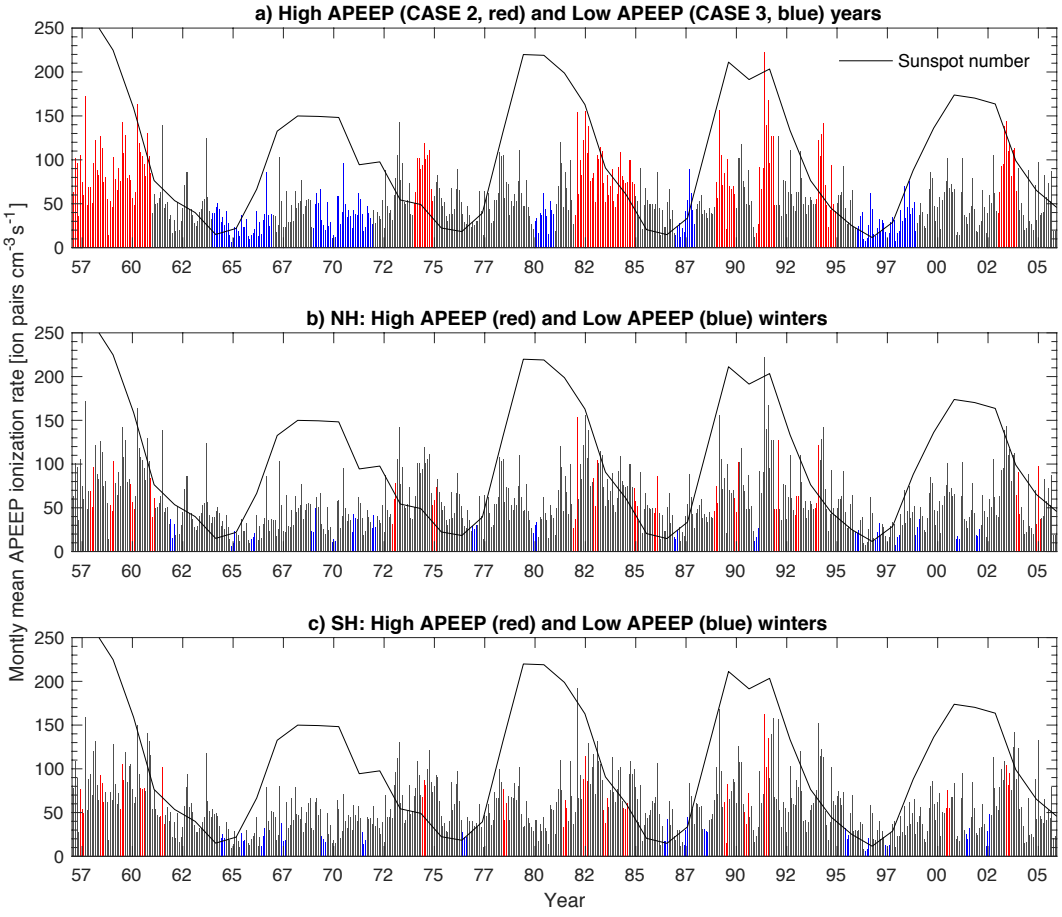

Figure 1. Monthly mean ionization rates at 77 km altitude and L-shell range 3.25–10 (magnetic latitude 55–72°) from the APEEP model. The black line is the annual mean sunspot number (values given on y-axis) indicating the progression of the 11-year solar cycle. a) Red and blue bars indicate years of high MEE (CASE 2) and low MEE (CASE 3) as in Table 1, respectively. b) Red and blue bars indicate high and low MEE winters in the Northern Hemisphere (see Table 2), respectively. c) Same as b) but for the Southern Hemisphere (see Table 2).

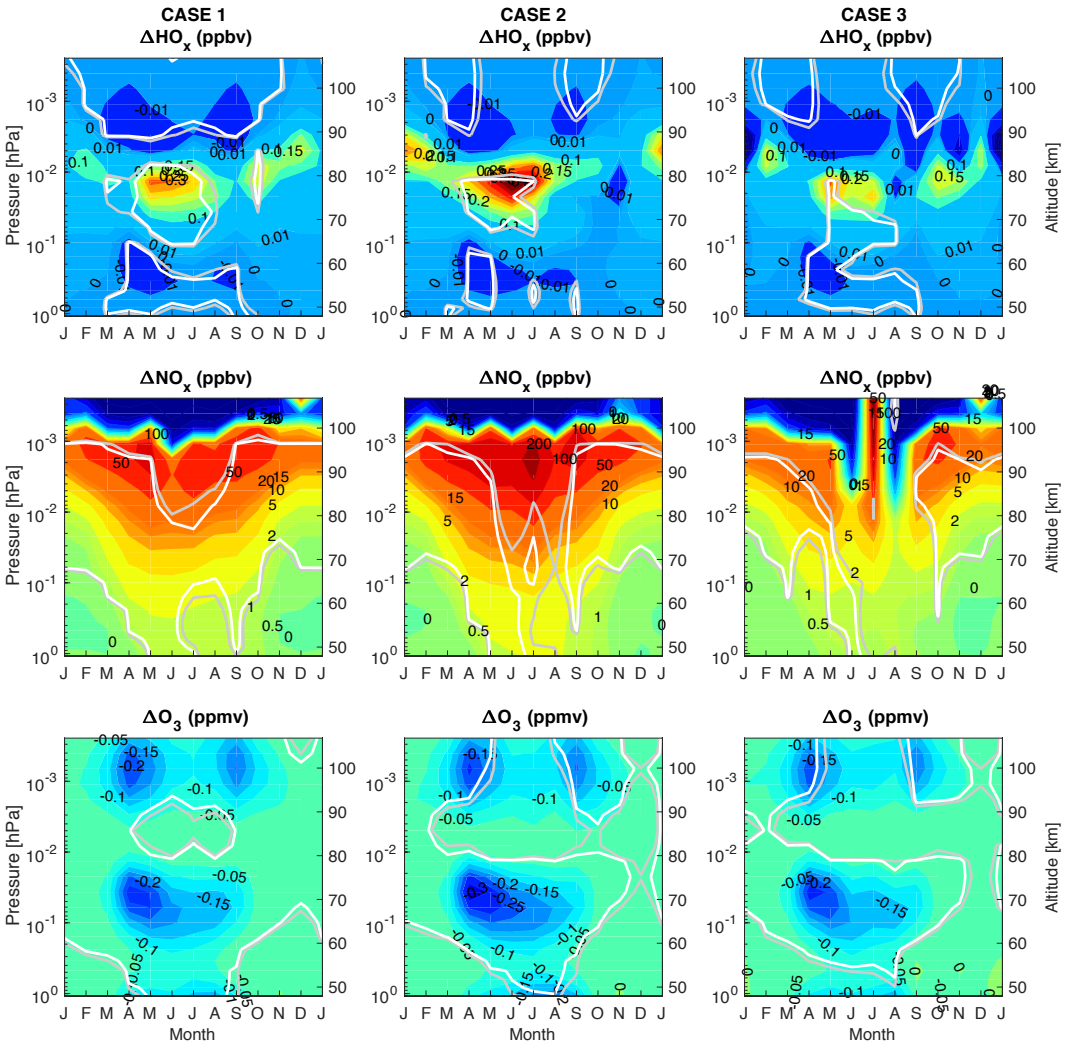

Figure 2. Monthly mean polar SH (60–90°S) HO_x (top, ppbv), NO_x (middle, ppbv) and O_3 (bottom, ppmv) composite difference "MEE_CMIP5 – REF_CMIP5". The data are from all ensemble members for CASE 1 (left panel, all years), CASE 2 (middle, High APEEP ionization), and CASE 3 (right, Low APEEP ionization). The gray and white contours represent the 90% and 95% confidence levels respectively. Note that winter months are in the middle of the x-axis.

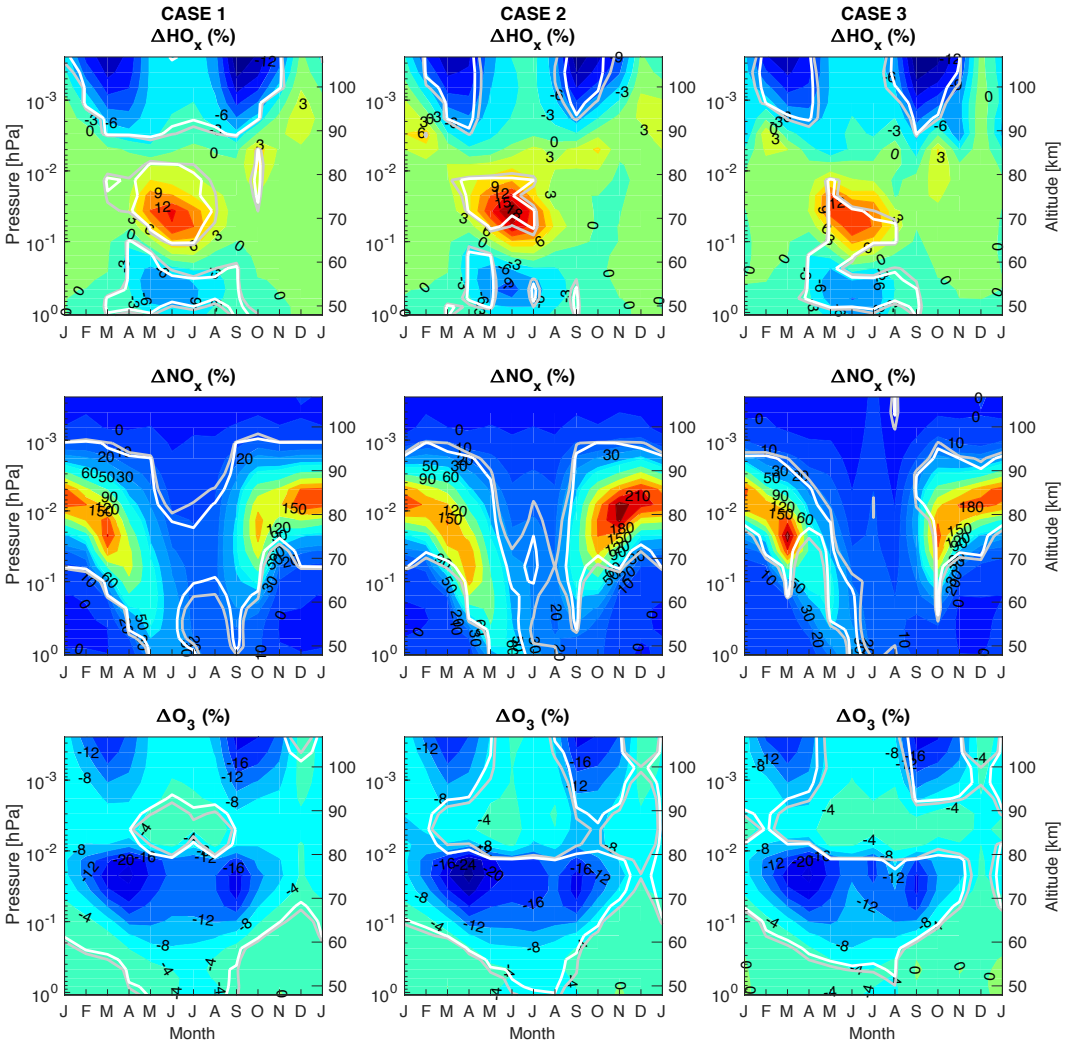

709 **Figure 3.** Same as Figure 2 but in relative to the REF_CMIP5 results (%-change).

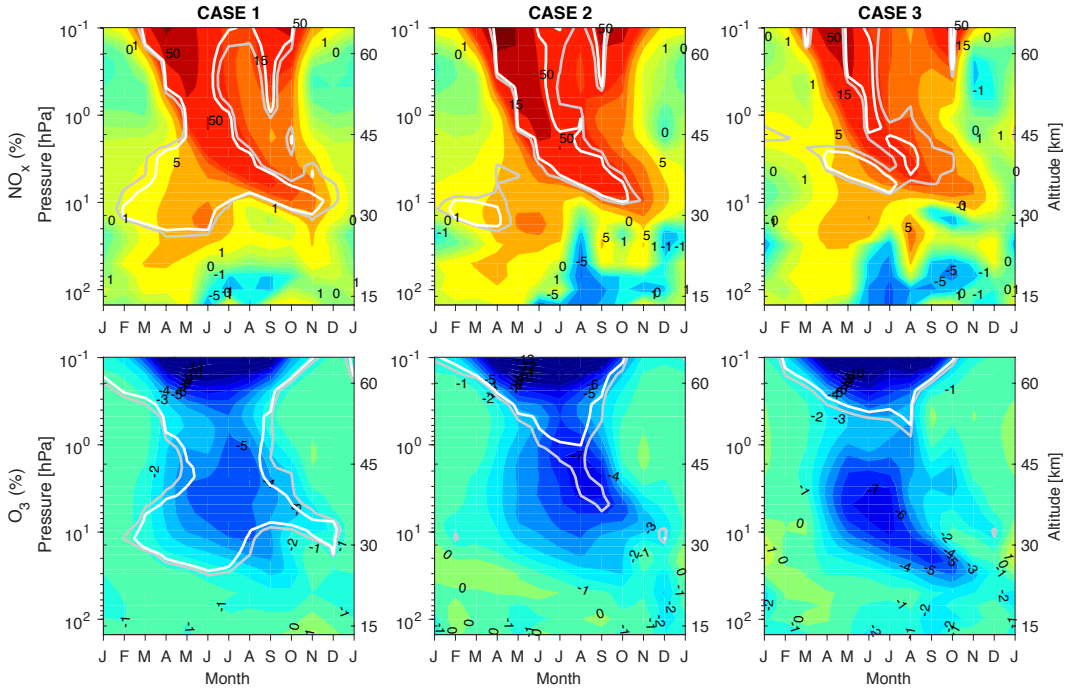

Figure 4. Monthly mean NO_x (top panels) and O_3 (bottom panels) response to the ionization from the APEEP model, calculated as percent of the composite difference "MEE_CMIP5 – REF_CMIP5". The data are from the SH, averaged over latitudinal range 60–90°S and over all ensemble members for CASE 1 (left, all years), CASE 2 (middle, High APEEP ionization), and CASE 3 (right, Low APEEP ionization). The gray and white contours represent the 90% and 95% confidence levels respectively.

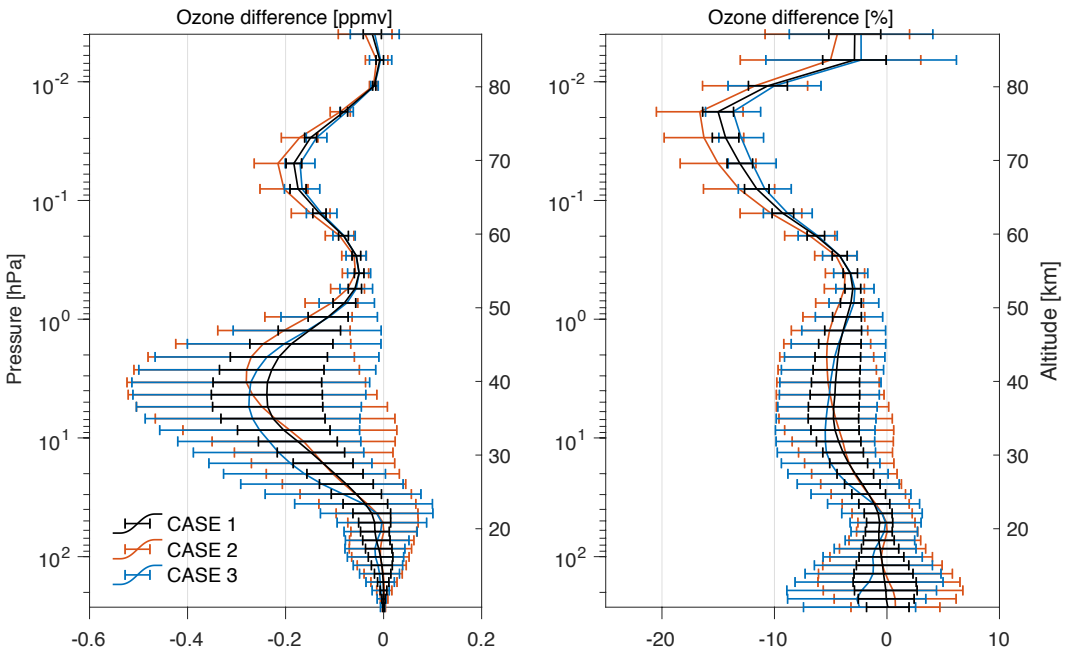

Figure 5. SH winter (June–August) zonal mean O_3 response to the ionization from the APEEP model, calculated as difference between the MEE_CMIP5 and REF_CMIP5 simulations. The data were averaged over the latitudinal range 60–90°S and over all ensemble members. Horizontal bars indicate the standard error of the mean (SEM) of the difference (see text for details).

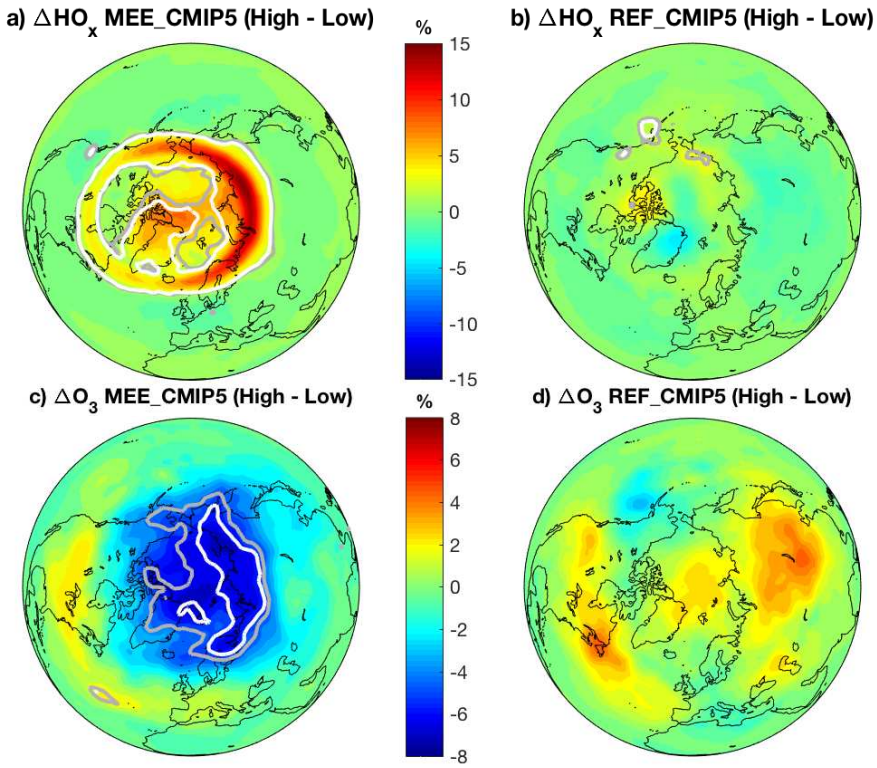

719 **Figure 6.** NH winter (December–January–February) "High EPP – Low EPP" composite HO_x (top) and O_3
720 (bottom)%-differences for the MEE_CMIP5 simulation (left) and REF_CMIP5 simulation (right) in the upper
721 mesosphere at 70–80 km altitude. The gray and white contours represent the 90% and 95% confidence levels,
722 respectively. For list of years in each composite group see Table 2.

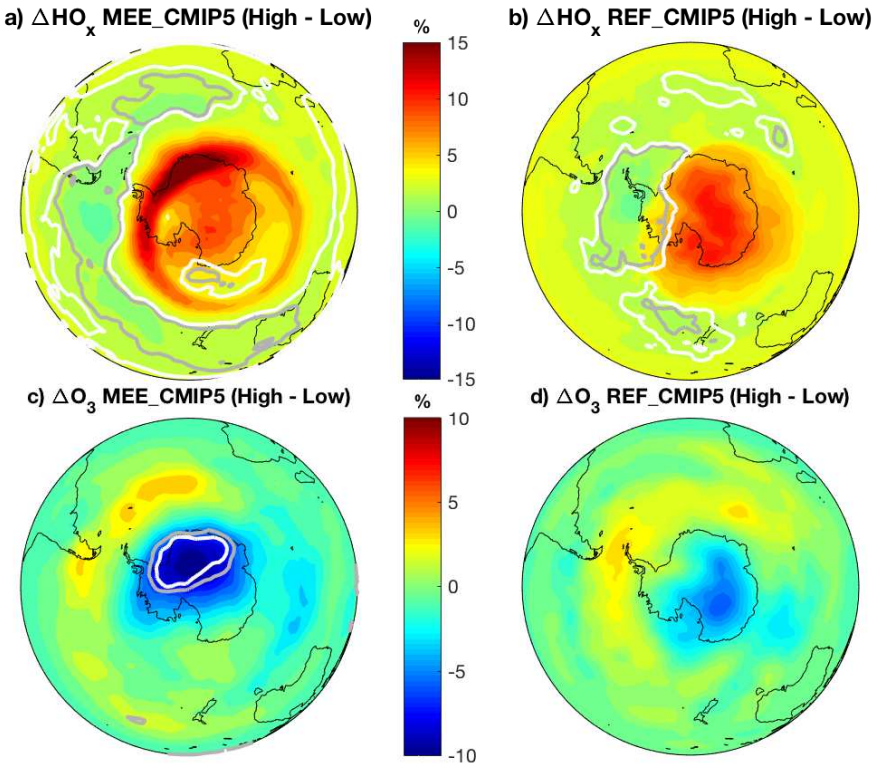

723 **Figure 7.** As Figure 6, but for SH winter (June–July–August).

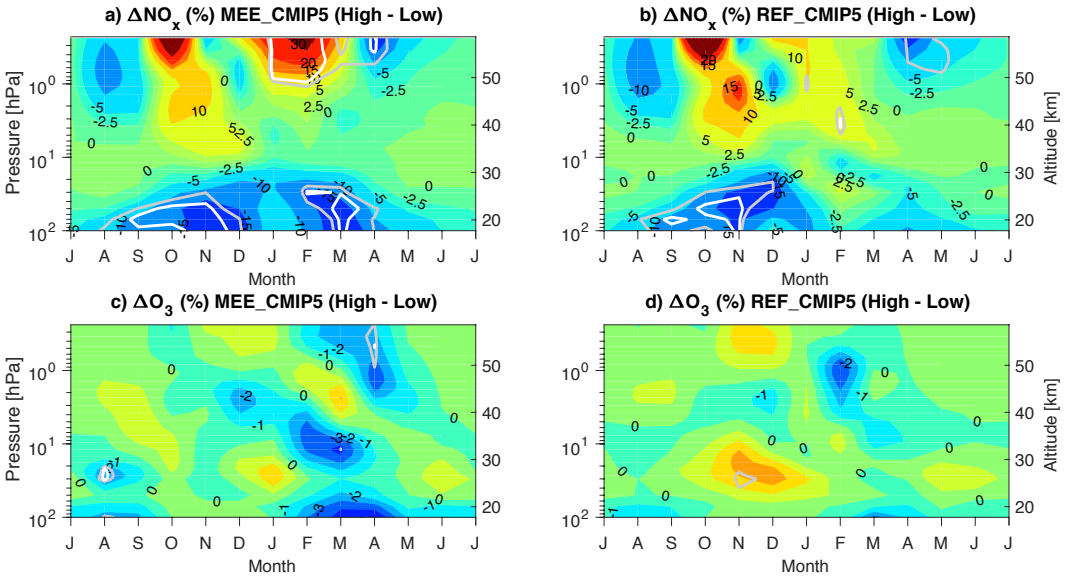

724 **Figure 8.** Monthly mean NH polar (70°–90°N) EPP-driven NO_x (top) and ozone (bottom) variability:
725 "High EPP – Low EPP" (shown as %-difference). Left: MEE_CMIP5 simulation. Right: REF_CMIP5 sim-
726 ulation. The gray and white contours represent the 90% and 95% confidence levels, respectively. For list of
727 years in each composite group see Table 2. The early winter NO_x enhancement visible on both experiments is
728 a result of the Halloween 2003 SPEs being included in the total EPP forcing for "High EPP" years. Note that
729 winter months are in the middle of the x-axis to ease comparison with Figure 9.

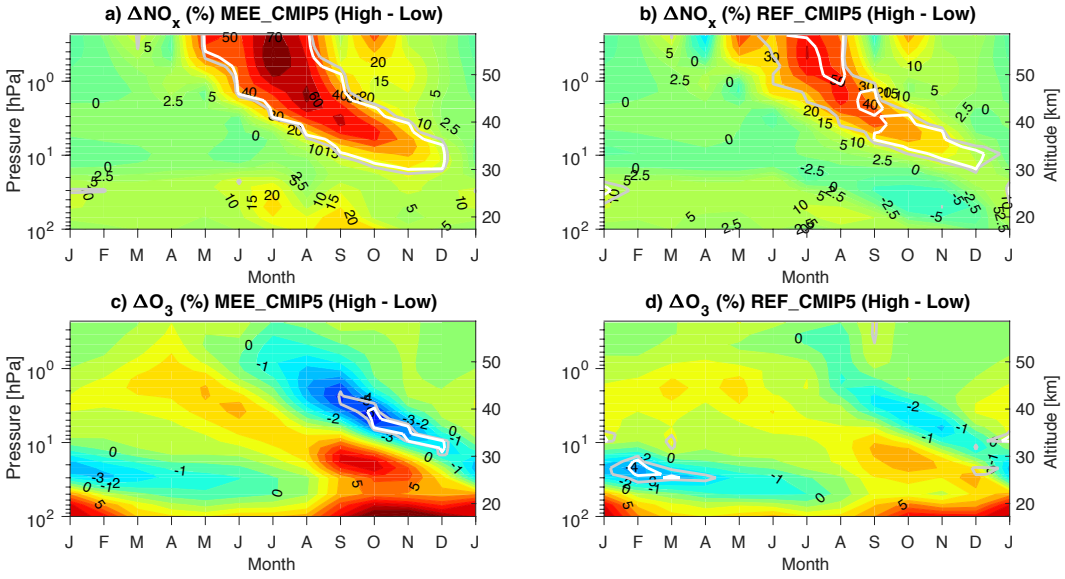

730 **Figure 9.** As Figure 8 but for the SH (60°–90°S). For list of years in each composite group see Table 2.